SPIE Conf. Proc.: Smart Structures and Materials 2005: Behavior and Mechanics, March, 2005, San Diego, CA

Characterization of Ternary NiTiPt High-Temperature Shape Memory Alloys

Orlando Rios[a], Ronald Noebe[b], Tiffany Biles[b], Anita Garg[b], Anna Palczer[b], Daniel Scheiman[b], Hans Jürgen Seifert[a], Michael Kaufman[c]
[a]Department of Materials Science and Engineering, University of Florida, Gainesville, FL
[b]NASA Glenn Research Center, Cleveland, OH
[c]Department of Materials Science and Engineering, University of North Texas, Denton, TX

ABSTRACT

Pt additions substituted for Ni in NiTi alloys are known to increase the transformation temperature of the alloy but only at fairly high Pt levels. However, until now only ternary compositions with a very specific stoichiometry, $Ni_{50-x}Pt_xTi_{50}$, have been investigated and then only to very limited extent. In order to learn more about this potential high-temperature shape memory alloy system, a series of over twenty alloys along and on either side of a line of constant stoichiometry between NiTi and TiPt were arc melted, homogenized, and characterized in terms of their microstructure, transformation temperatures, and hardness. The resulting microstructures were examined by scanning electron microscopy and the phase compositions quantified by energy dispersive spectroscopy. "Stoichiometric" compositions along a line of constant stoichiometry between NiTi to TiPt were essentially single phase but any deviations from a stoichiometry of $(Ni,Pt)_{50}Ti_{50}$ resulted in the presence of at least two different intermetallic phases, depending on the overall composition of the alloy. Essentially all alloys, whether single or two-phase, still under went a martensitic transformation. It was found that the transformation temperatures were depressed with initial Pt additions but at levels greater than 10 at.% the transformation temperature increased linearly with Pt content. Also, the transformation temperatures were relatively insensitive to alloy stoichiometry within the range of alloys examined. Finally, the dependence of hardness on Pt content for a series of $Ni_{50-x}Pt_xTi_{50}$ alloys showed solution softening at low Pt levels, while hardening was observed in ternary alloys containing more than about 10 at.% Pt. On either side of these "stoichiometric" compositions, hardness was also found to increase significantly.

1. INTRODUCTION

Due to its superior shape memory and superelastic behavior, NiTi alloys have found diverse commercial use in such applications as electrical switches, eyeglass frames, brassiere underwires, cell phone antennas, appliance controllers, temperature sensitive valves, microactuators, and countless medical and dental devices.[1,2] In addition, the first large-scale commercial applications for shape memory alloys were for NiFeTi and NiNbTi alloys with sub-room temperature transformation temperatures, for use as couplings for pipes, tubes, and electrical interconnects.[1,3] But all of these applications represent the use of NiTi alloys near room temperature. The reason that applications have been limited to this narrow range of temperatures is that conventional NiTi shape memory alloys (SMA) have a maximum transformation temperature of about 100 °C.

There should be many additional control and actuation-type applications, for materials exhibiting shape memory behavior at high temperatures. For instance, high-temperature shape memory alloys (HTSMA) would find widespread use in the aeronautic, automotive, power generation, and chemical processing industries. But even though many specific applications have been identified and countless patents exist for the design of high-temperature devices based on some form of a HTSMA, there are no commercially available materials with mechanical and shape memory properties similar to NiTi but with significantly elevated transformation temperatures.

In the past few years, many research groups have started to investigate HTSMA based on ternary NiTiX compositions. Several alloys including those based on (Ni,Pd)Ti, (Ni,Au)Ti, (Ni,Pt)Ti, Ni(Ti,Hf) and Ni(Ti,Zr) that have been shown to exhibit high transformation temperatures and thermal shape memory effects have recently been reviewed.[4] Of these systems, the (Ni,Au)Ti and (Ni,Pt)Ti have the highest potential use temperatures but have been the least studied.

Lindquist and Wayman[5] have shown that alloying NiTi with Pt raises the martensitic transformation temperature of NiTi quite significantly and a few room temperature tensile tests have been performed by Hosoda et al.[6] But little else has been published on this system. Consequently, this study was initiated to focus on the compositional dependence of the microstructural, thermal, and mechanical properties of the high temperature Ni-Ti-Pt SMA system.

2. EXPERIMENTAL OVERVIEW

A set of over twenty target compositions were chosen in order to survey the basic properties of the Ni-Ti-Pt system close to the line of constant stoichiometry between NiTi and TiPt, in a region where one would expect to find potential high-temperature shape memory behavior. The experimental alloys were produced by vacuum, non-consumable-arc melting of high purity starting components (99.95 Ti, 99.995Pt, 99.98Ni) using a water cooled copper crucible. Since the density difference between the starting materials was large and could result in an inhomogeneous suspension of unmixed components, the buttons were turned over and remelted 4-6 times to insure homogeneity. The arc melted buttons were then homogenized in a vacuum furnace for 72 hr at 1050 °C and allowed to furnace cool. The heating rate was controlled and the furnace's hot zone was measured in order to verify that no gross temperature gradients existed within this region. Cursory sample evaluations revealed no major surface oxidation.

Samples for DSC, DTA, metallography, and chemical analysis were machined from the arc melted buttons by wire EDM. Pieces for metallographic examination were mounted in phenolic bond pressure mounts and subsequently polished by automated procedures identified for these materials. The DTA samples consisted of 5 mm diameter by 10 mm long cylinders; and 5mm diameter by 1 mm thick disks were used for DSC analysis. The bulk alloy compositions were determined by inductively coupled plasma spectroscopy and the measured results are compared to the original aim compositions in Table 1. Impurity concentrations were also determined using standard LECO O/N and C/S Determinators and are also reported in Table 1.

Vickers microhardness testing was performed on the mounted and polished samples in accordance with the ASTM standard for metallic materials.[7] At least 10 measurements were taken at random locations within the interior section of the sample, in order to yield a statistically significant mean hardness.

SMA's are characterized by a set of temperatures at which a crystallographic structural change begins and ceases. These are defined as A_s, A_f, M_s and M_f. The A_s temperature is a temperature at which the transformation of the martensite to austenite phase begins. A_f is the temperature at which the transformation is completed and the material is 100% austenite. M_s and M_f are the temperatures at which the reverse transformation occurs.[8] A TA Instruments DSC Q1000 and a Netzsch 409 thermal analyzer DTA were used for thermal analysis to determine these transformation temperatures. Transformation temperatures were determined by differential scanning calorimetry (DSC) for low to intermediate temperature analyses and differential thermal analysis (DTA) was used at intermediate to high temperatures, since the DSC was limited to about 300 °C in operating temperature. For both techniques, a heating and cooling rate of 10 °C per min was used. Data analysis was performed using the TA Universal Analysis 2000 Software package.

The sectioned and polished alloys were examined using a JEOL 6400 scanning electron microscope (SEM) using back scattered electron (BSE) mode. An annular detector was used in order to maximize the signal. The sample surfaces were kept normal to the 15 KeV beam and parallel to the detector's exposed face. This configuration maximizes phase contrast and minimizes any topographical effects. All comparable imaging was done at the same magnification in order to allow for simple sample comparisons. Semi-quantitative ZAF corrected EDS analysis of the various phases was performed using the NiK_α, TiK_α, and PtM_α lines.

3. RESULTS AND DISCUSSION

3.1 Bulk chemical analysis

The resulting experimental alloy compositions are graphically represented on the Gibb's triangle shown in Figure 1. The alloys were categorized into three classes. "Stoichiometric" alloys were located along the line defined by $Ni_{50-x}Pt_xTi_{50}$. This set of alloys is used for comparison to the previous work by Lindquist and Wayman and for comparison to the so-called non-stoichiometric alloys. The second category of materials is a subset of two of these stoichiometric

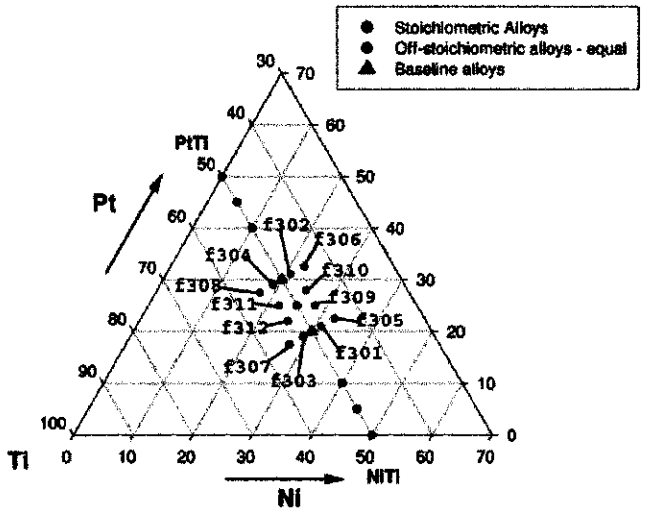

Figure 1. Ternary plot of the Ti-Ni-Pt compositions studied. The composition of all alloys was confirmed by spectrographic analysis

Table 1. Aim and measured compositions of all alloys investigated in this study

	Aim Composition (at.%)			Measured Compositions (at.%)					
sample designation	Ti	Ni	Pt	Ti	Ni	Pt	C	N	O
E426	50	50	0	49.96	49.73	0	0.05	0.01	0.18
E427	50	45	5	49.86	45.13	4.58	0.08	0.01	0.26
E428	50	40	10	50.02	40.01	9.66	0.06	0.02	0.17
E429	50	30	20	49.43	29.52	20.64	0.07	0.02	0.25
E430	50	25	25	49.88	25.25	24.48	0.07	0.02	0.22
E431	50	20	30	49.77	20.03	29.81	0.08	0.03	0.21
E432	50	10	40	49.83	9.78	39.94	0.07	0.02	0.24
E433	50	5	45	49.94	5.04	44.53	0.11	0.03	0.23
E434	50	0	50	49.9	0	49.48	0.08	0.04	0.3
F301	48	31	21	48.02	31.01	20.45	0.12	0.08	0.28
F302	48	21	31	47.79	20.79	30.79	0.11	0.12	0.36
F303	52	29	19	52.03	29.01	18.5	0.09	0.07	0.23
F304	52	19	29	51.58	19.38	28.52	0.13	0.09	0.25
F305	45	32.5	22.5	45	32.27	22.35	0.05	0.05	0.25
F306	45	22.5	32.5	44.84	22.76	31.87	0.076	0.05	0.3
F307	55	27.5	17.5	54.02	28.26	17.16	0.08	0.08	0.37
F308	55	17.5	27.5	54.46	18.23	26.73	0.1	0.108	0.23
F309	47	28	25	46.81	27.89	24.77	0.11	0.09	0.27
F310	47	25	28	47.05	25	27.43	0.11	0.08	0.25
F311	53	22	25	52.58	22.35	24.49	0.13	0.1	0.29
F312	53	25	22	52.59	25.08	21.68	0.12	0.09	0.38
F313	48	21	31	38.79	25.24	35.54	0.09	0.07	0.2

compositions that have been chosen as base-line alloys for detailed mechanical testing. The results of that study are included in these proceedings.[9] Selection of these base-line alloys was based on previous review of the literature combined with preliminary mechanical testing that suggested these compositions were capable of shape memory behavior. Finally, a set of non-stoichiometric alloys was cast in order to determine the effects of stoichiometry on the mechanical properties, microstructure, and especially the transformation temperatures of these materials.

3.2 Microstructural and semi-quantitative EDS analysis

As expected, all the stoichiometric alloys were essentially single phase. These alloys are designated by the prefix E in Table 1. Micrographs of these alloys were omitted as they did not provide any useful information other than essentially confirming the single phase nature of the microstructure.

Conversely, most of the non-stoichiometric alloys, designated by the prefix F, were found to contain a second phase. Figure 2 is a summary of the microstructures for all the F-series alloys. Referring to this figure, samples F303 and F304 are essentially single-phase non-stoichiometric alloys, in that they do not contain a second intermetallic phase. The spherical dark phase in these alloys is probably TiO_2, which is common to all the alloys. The microstructure for these two alloys is similar to that observed in the E-designated alloys. F303 is comparable to the microstructure of the lower Pt E-series alloys where the martensite is finely distributed and F304 is similar to the higher Pt E-series alloys with a coarse distribution of martensite.

The fact that most of the alloys contain second phases, even very close to the line of constant stoichiometry, indicates that the solubility of excess alloying additions on either side of this line is very narrow, especially on the (Ni+PT)-rich side. The only two non-stoichiometric alloys that did not contain a second intermetallic phase were observed on the Ti-rich side of this line of constant stoichiometry. However, both of these alloys contained Ti-rich interstitial containing phases. Given the overall composition of the alloys (Table 1), these were probably oxides. Therefore, any excess Ti could be tied up as TiO_2 and the bulk matrix phase was probably very close to a stoichiometric composition. Consequently, there is probably little solubility for excess solute on either side of stoichiometry.

Additionally, analysis of the microstructures revealed that sample F307 underwent incipient melting at the grain boundaries during the homogenization treatment, indicating the possible formation of Ti_2Ni which is a Ti rich low melting point phase shown in the Ti-Ni binary phase diagram reproduced for convenience in Figure 3. The evidence of incipient melting is in the morphology of the grains and the fine microstructure of the Ti-rich grain boundaries. As a result the thermal and mechanical data from this sample were not included in any of the additional analyses.

The different phases in the F-series alloys, shown in Figure 2, are indicated by an arrow and labeled with a number "1" or "2". Phases marked as "1" are the martensitic or parent phase while phases marked as "2" are the second phase. EDS was performed for each of these phases and the ZAF corrected EDS quantitative results are summarized in Table 2. Possible phase identifications for the second phases were based on compositional information determined by EDS as compared with the published phase diagrams for the two binary systems,[10,11] which are provided in Figures 4 and 5. Both phase diagrams are recent assessments of the respective binary system.

Based on the compositional analysis (Table 2) and basic morphology of the microstructures (Figure 2), there are basically two types of second phases observed in the non-stoichiometric alloys. All the (Ni+Pt)-rich alloys contain a lathe like structure with a 2:3 Ti:(Ni+Pt) ratio. Given the nature of this phase, it would appear that it forms by nucleation in the solid state. An intermetallic phase with the stoichiometry of $Ti_2(Ni,Pt)_3$ does not appear in either binary phase diagram, however, Ti_2Ni_3 is a metastable phase that is observed in binary NiTi alloys. Consequently, the Pt could stabilize this phase. Or it is possible that it is a new phase, unique to the ternary phase diagram. It will take additional quantitative x-ray diffraction or TEM analysis to determine the specific structure of this phase.

The non-stoichiometric alloys on the Ti-rich side of the line of constant stoichiometry, have a phase that is more spherical or elliptical in morphology and usually located along the grain boundaries. This would indicate that it is possibly a low melting point phase that was last to form during solidification. This and the fact that the composition has a 2:1 Ti:(Ni,Pt) ratio, would indicate that it could be $Ti_2(Ni,Pt)$, which is isostructural to Ti_2Ni and has been previously identified by Garg.[12] A small percentage of other phases may also appear in these alloys.

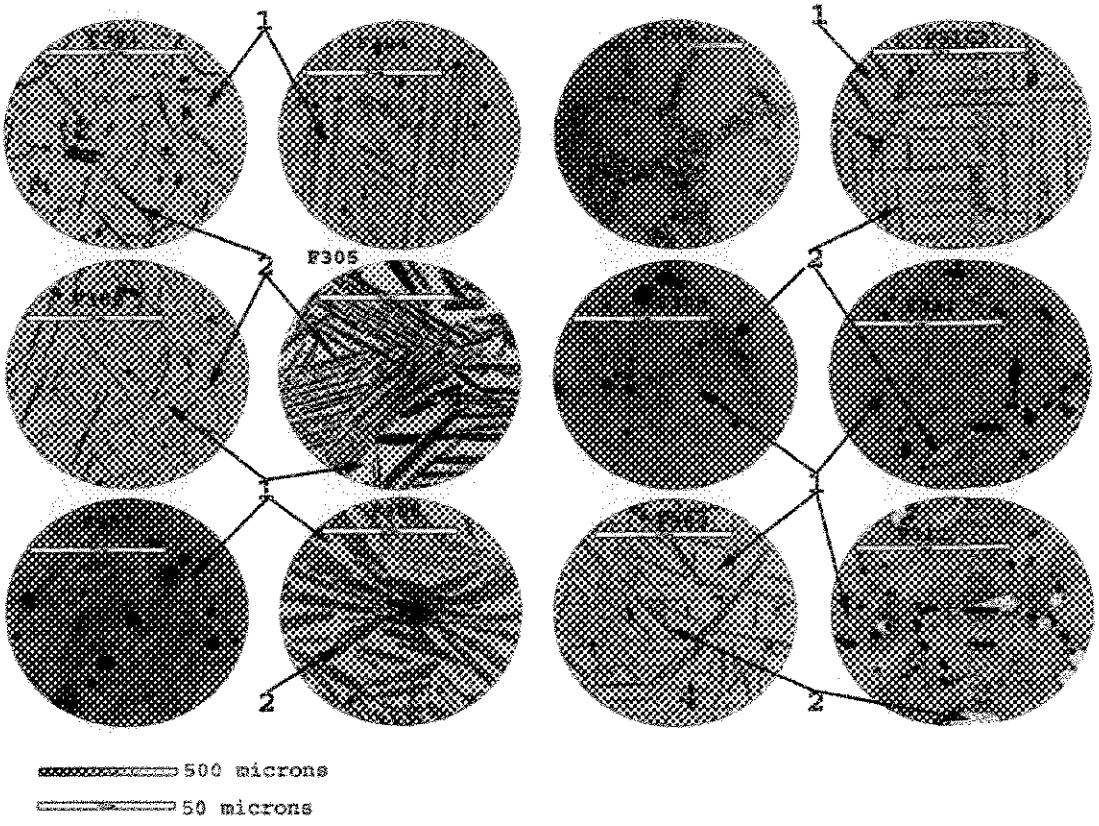

Figure 2. SEM BSE micrographs of the non-stoichiometric alloys.

Table 2. Semi-quantitative EDS analysis of the various phases observed

Sample ID	Bulk Composition (at.%)			Region 1 (martensite) (at.%)			Region 2 (second phase particle) (at.%)		
	Ti	Ni	Pt	Ti	Ni	Pt	Ti	Ni	Pt
F301	48.02	31.01	20.45	46.46	29.01	24.53	39.44	38.67	21.89
F302	47.79	20.79	30.79	46.53	17.79	35.69	39.16	29.46	31.38
F303	52.03	29.01	18.5	49.43	28.22	22.35			
F304	51.58	19.38	28.52	48.46	18.25	33.3			
F305	45	32.27	22.35	47.3	22.87	29.82	39.15	34.65	26.2
F306	44.84	22.76	31.87	45.7	15.35	38.95	38.81	27.38	33.81
F308	54.46	18.23	26.73	47.04	22.08	30.89	62.98	8.94	28.08
F309	46.81	27.89	24.77	45.36	25.35	29.29	43.74	27.84	28.42
F310	47.05	25	27.43	46.3	20.63	33.08	44.78	24.37	30.85
F311	52.58	22.35	24.49	49.76	21.11	29.13	66.6	1.67	31.74
F312	52.59	25.08	21.68	48.9	26.97	24.13	67.19	2.37	30.44

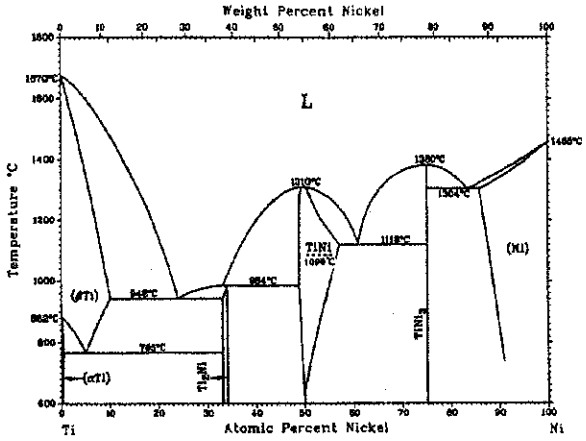

Figure 3. NiTi binary phase diagram from reference (10).

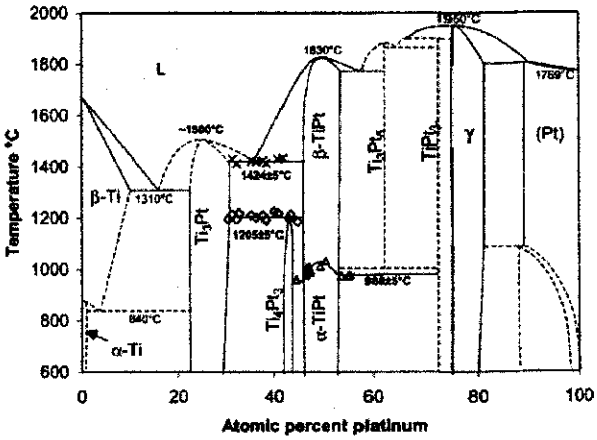

Figure 4. TiPt phase diagram from reference (11)

3.3 Thermal behavior

Thermal analysis of the transformation temperatures was determined by DSC or DTA for each sample. An example of the thermal data is shown in Figure 5, which are the DTA results for the Ni-25Pt-50Ti sample (E250). As labeled in the plot, exothermic effects are plotted in the positive direction. In the heating cycle, austenitic transformations have a strong characteristic endothermic peak while martensitic reactions have a strong exothermic peak. The values of the transformation temperatures are defined at the extrapolated onset or endpoint of the martensitic or austenitic transformation peaks.[13] For example, the extrapolated peak onset temperature is the point of intersection of the tangent drawn on the leading edge of the peak with the extrapolated baseline.

A complete set of results from the thermal analyses is contained in Table 3. All the samples were run through at least two cycles in order to stabilize the transformation temperatures. The reported values come from the second thermal cycle. Subsequent cycles on these alloys did not significantly affect the transformation temperatures any further, signifying that the transformation dynamics were relatively stable at this point.

This study was initially designed to build strong compositional based relationships between the transformation thermodynamics and mechanical properties, therefore requiring the analysis of the multidimensional data acquired in this experimental set. Consequently, MathCAD was implemented in the generation of a series of scatter plots and a series of contour plots based on the thermal data in Table 3 and the hardness data described in the next section.

A transformation scatter plot is shown in Figure 6. The XY plane represents the compositional coordinates of each sample. In this plane the compositions of the Pt and Ti are represented while the representation of the Ni compositions is implied, since at.%Pt + at.%Ti + at.%Ni = 100. Figure 6 shows the distribution of data points used to generate the compositional dependent transformation temperature surfaces. Contour plots were generated based on the extrapolated surface mesh. Figure 7 is a contour plot of the austenite start and finish temperatures as a function of composition. Similarly, Figure 8 is a contour plot of the martensite start and finish temperatures. Small substitutions of Pt for Ni initially cause a slight depression in the transformation temperatures as evident in the lower temperature contours. In Figures 7 and 8 the lower temperature contours bend into the higher Pt compositions, particularly in the stoichiometric alloys. This suppression in transformation temperature has been reported previously by Lindquist and Wayman for stoichiometric $Ni_{50-x}Pt_xTi_{50}$ alloys and is in excellent agreement with our data as shown in Figure 9. However, there is some discrepancy at 10 at.% Pt. Since Lindquist and Wayman performed their thermal analysis by examining the alloys resistivity as a function of temperature, this could possibly lead to a disparity between their data and the DSC data due to differences in the methods used to determine the transformation temperatures. Transformation temperature determination is performed by the peak onset method for the DSC technique while from resistivity curves the transformation temperatures are defined at the intersection of the extrapolated linear regions. As a result the transformation temperatures determined by resistivity measurements are dependent on the curve morphology.

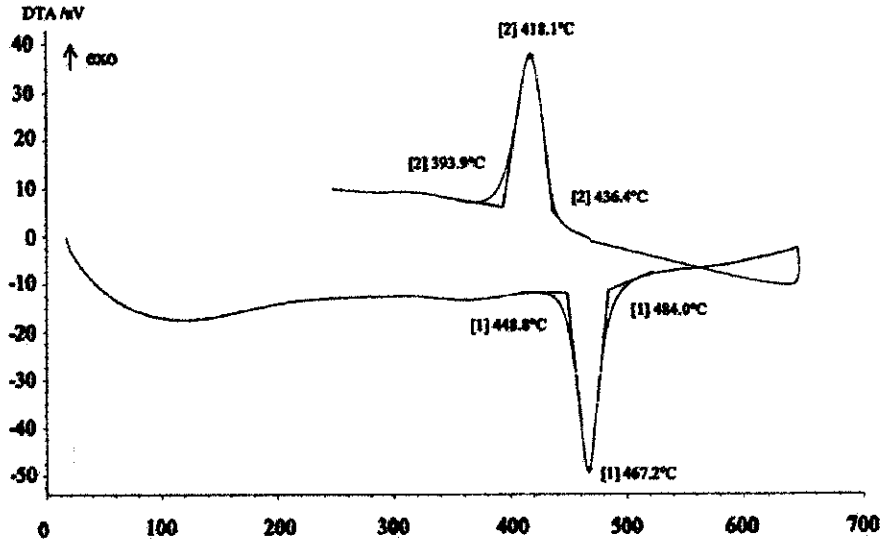

Figure 5. DTA results for sample E250 (Ni-25Pt-50Ti)

Table 3. Transformation temperatures and sample hardness.

Sample designation	A_s (°C)	A_f (°C)	M_s (°C)	M_f (°C)	Hv
E246	60	86	57	35	194
E247	51	65	46	25	164
E248	86	94	87	76	146
E249	313	322	312	296	246
E250	449	484	436	394	266
E251	600	653	591	527	271
E252	838	917	811	751	342
E253	963	998	917	869	348
E254	1044	1069	1018	996	243
F301	284	352	307	239	310
F302	666	780	605	552	384
F303	268	302	259	212	256
F304	526	560	492	424	317
F305	444	511	459	379	344
F306	no peaks				380
F308	486	519	470	423	352
F309	449	507	446	382	378
F310	552	617	523	468	303
F311	420	453	402	363	319
F312	342	374	286	330	367

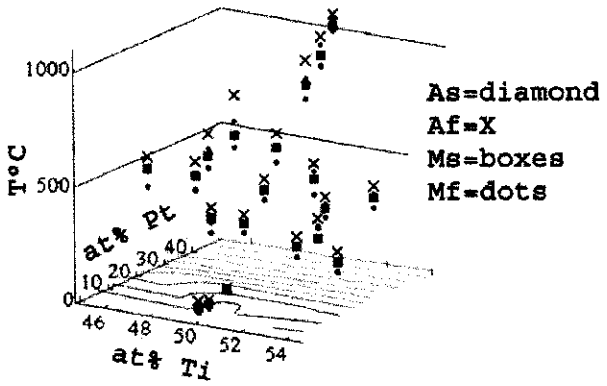

Figure 6. Multidimensional composition dependent transformation scatter plot with base contour plot.

In their study, Lindquist and Wayman showed that the curve morphology was strongly sensitive to alloy composition possibly leading to the differences in the reported transformation temperature values. Finally, an effect which is not clearly evident in the contour plot is the widening of the transformation hysteresis with increasing Pt content, or higher transformation temperatures (Figure 10).

Figures 7 and 8 are functional working maps for transformation temperature based alloy development near the experimental compositions. These contour plots can be used to determine compositional dependent transformation temperature trends exhibited by this system and have a high degree of accuracy since they represent extrapolations between actual data.

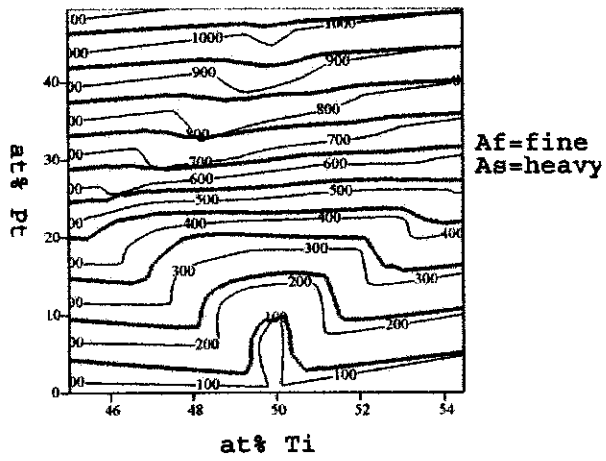

Figure 7. Austenitic transformation contour plot mapping the compositional dependence of the austenite start and finish temperatures.

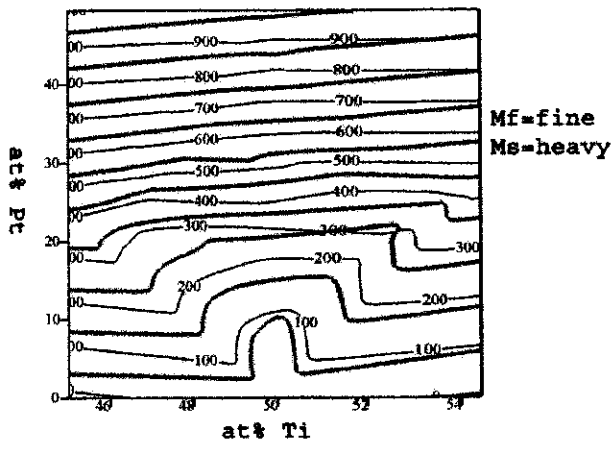

Figure 8. Martensitic transformation contour plot mapping the compositional dependence of the martensite start and finish temperatures.

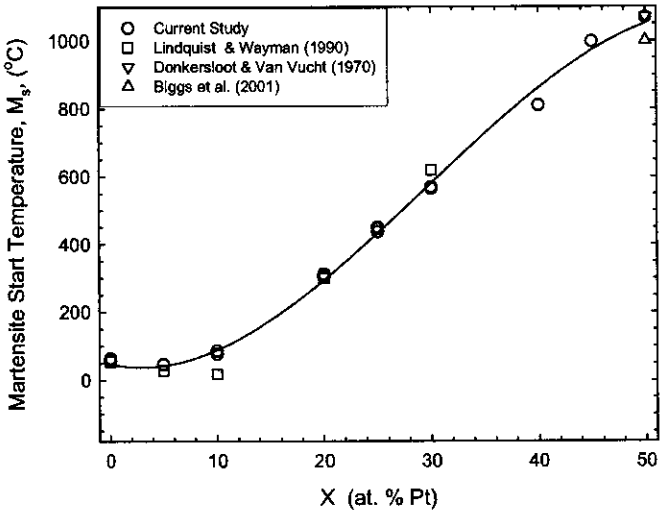

Figure 9. Effect of Pt on the M_s transformation temperatures for $Ni_{50-x}Pt_xTi_{50}$ alloys, including data from previous researchers[5,14,15].

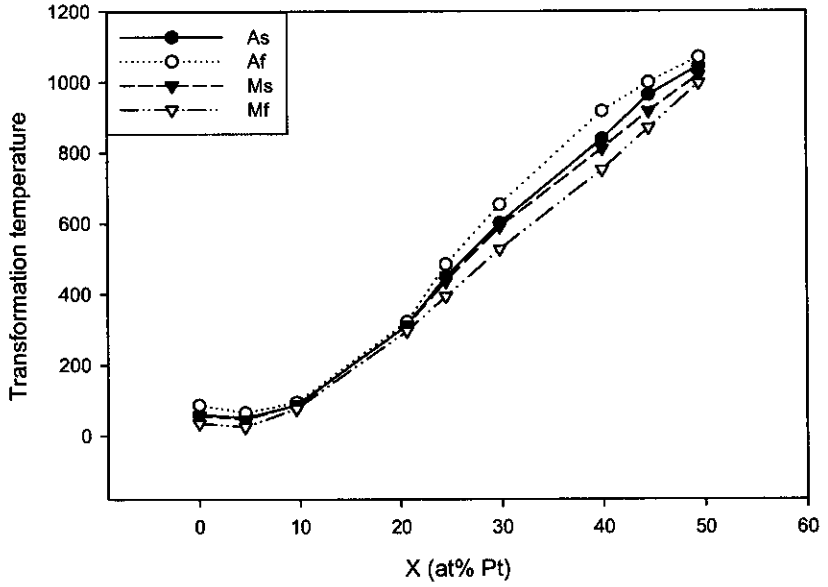

Figure 10. Effect of Pt on all transformation temperatures for $Ni_{50-x}Pt_xTi_{50}$ alloys.

3.4 Mechanical Hardness Testing

The recorded mean Vickers hardness (H_v) values are listed in Table 3. In a similar fashion to the thermal data, a scatter plot was generated for the hardness values. This plot is shown in Figure 11. The resulting contour plot imposed on the X Y plane is shown in Figure 12. Finally, the dependence of hardness on Pt level for a series of $Ni_{50-x}Pt_xTi_{50}$ alloys is shown in Figure 13. At Pt levels up to about 10 at.%, solution softening was observed while for higher Pt levels solid solution hardening occurred. This is actually comparable to the thermal behavior exhibited by the stoichiometric alloys.

As seen in Figure 12, deviations from stoichiometry strongly affect hardness. Slight compositional shifts increase the hardness of these alloys a significant amount. Further deviations result in the formation of an increasing amount of second phase which does not increase the hardness as strongly. It is possible that the increase in hardness may be due to solid solution hardening and defects which form to maintain stoichiometry in this highly ordered structure as much as it is due to any second phase.

Pt additions in excess of 10 at% were shown to harden the martensite as well as widen the thermal hysteresis. It has been shown in a study by Ortin and Planes[16] that constraining transformation strains increases the thermodynamic driving force, hence, the undercooling necessary to drive the transformation. In this system, strengthening of the martensite obstructs the transformation; hence, the observed widening of the hysteresis at the higher Pt contents.

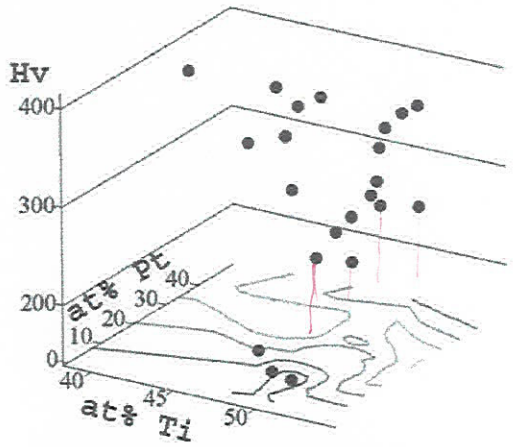

Figure 11. Multidimensional composition dependent transformation scatter plot with base contour plot.

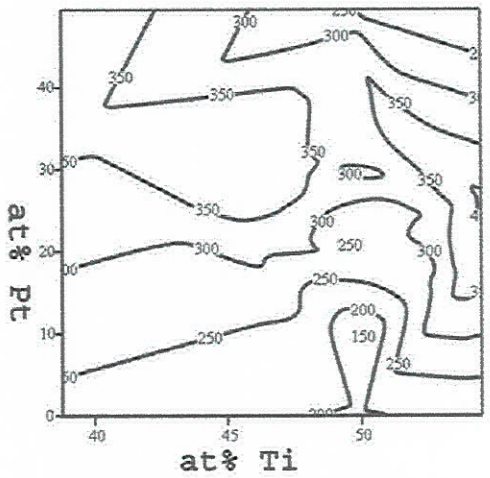

Figure 12. Hardness contour plot showing compositional dependence of hardness.

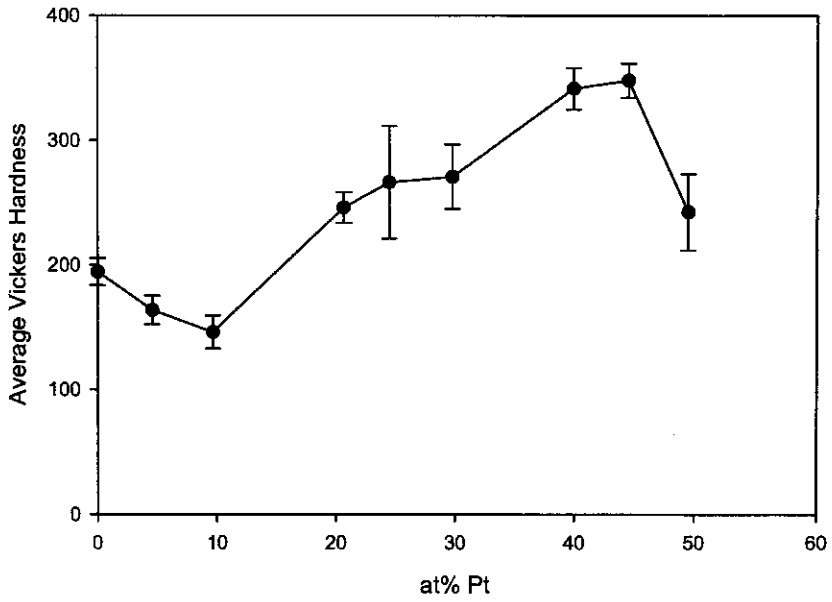

Figure 13. Effect of Pt content on the hardness of $Ni_{50-x}Pt_xTi_{50}$ alloys.

4. SUMMARY AND CONCLUSIONS

The microstructure, transformation temperatures, and hardness of a series of Ni-Ti-Pt alloys, at compositions expected to show high-temperature shape memory behavior have been studied. Non-stoichiometric compositions exhibited the formation of second phases. (Ni+Pt)-rich compositions contained precipitates with strong crystallographic orientation and a Ti:(Ni+PT) ratio of 2:3. At lower volume fractions and reasonable size, these precipitates could be beneficial for precipitation hardening and grain growth refinement. In this study the alloys were arc melted and given an extended homogenization heat-treatment, therefore, resulting in a course precipitate distribution. Proper mechanical processing and heat treatment could be used to form a finer precipitate distribution which may be used to strengthen the alloys as well as prevent excessive grain growth at elevated temperatures. The importance of strengthening the austenite phase in order to optimize the work output of high-temperature shape memory alloys was noted in the companion paper in this proceedings volume. Deviations on the Ti-rich side of stoichiometry do not appear to result in any apparently beneficial second phase, and instead results in the formation of a low melting point $Ti_2(Ni,Pt)$ phase along the grain boundaries.

The compositional based maps of transformation temperatures and hardness may be used as a starting point in further alloy development. From this set of maps, alloys based on Ni-Ti-Pt compositions may be tailored to fit specific design criteria. Although further mechanical testing is required to fully characterize each alloy and assess the effects of second phases on mechanical properties, the results presented here are useful as a guide to future alloy development. It is important to keep in mind that external conditions such as applied stress as well as the materials processing history will also affect the transformation temperatures. Subsequent studies will focus on exploring these dependencies.

ACKNOWLEDGEMENTS

The authors wish to thank Jami Olminsky for performing the compositional analyses and Joy Buehler for her assistance in the area of metallographic preparation. OR wishes to acknowledge the use of facilities at the Major Analytical Instrumentation Center, Department of Materials Science and Engineering, University of Florida. This work was supported by the Intelligent Propulsion Systems Foundation Technology Subproject of the Ultra-Efficient Engine Technology Project, Carolyn Mercer/Susan Johnson manager.

REFERENCES

1. T.W. Duerig, K.N. Melton, D. Stockel, and C.M. Wayman, *Engineering Aspects of Shape Memory Alloys*, Butterworth-Heinemann, Boston, 1990.
2. J. V. Humbeeck, "Non medical applications of shape memory alloys," *Maters. Sci. Eng.* **A273-275**, 134-148, 1999.
3. L. McD. Schetky, "The Industrial Applications of Shape Memory Alloys in North America", *Maters. Sci. Forum* **327-328**, 9-16, 2000
4. R.D. Noebe, T. Biles, S.A. Padula II, "NiTi-Based High-Temperature Shape-Memory Alloys: Properties, Prospects, and Potential Applications", in *Advanced Structural Materials*, ed. W.O. Soboyejo, Marcel Dekker, Inc, New York, 2005 (in press). (Also NASA TM 2004-213104).
5. P.G. Lindquist and C.M. Wayman, "Shape Memory and Transformation Behavior of Martensitic Ti-Pd-Ni and Ti-Pt-Ni Alloys," in *Engineering Aspects of Shape-Memory Alloys*, T.W. Duerig, K.N. Melton, D. Stockel and C.M. Wayman, Eds., Butterworth-Heinemann, Boston, (1990)
6. M. Hosoda, M. Tsuji, Y. Takahashi, T. Inamura, K. Wakashima, Y. Yamabe-Mitaria, S. Miyazaki, and K. Inoue, "Phase stability and mechanical properties of Ti-Ni alloys containing platinum group metals," *Maters. Sci. Forum* **426-432**, 2333-2338, 2003.
7. *ASTM Standard E 384 – 99*, "Standard Test Method for Microindentation Hardness of Materials."
8. C.M. Wayman and T.W. Duerig, "An Introduction to Martensite and Shape Memory," in *Engineering Aspects of Shape Memory Alloys*, T.W. Duerig, K.N. Melton, D. Stockel, and C.M. Wayman, eds., pp. 3-20, Butterworth-Heinemann, Boston, 1990.
9. R. Noebe, D. Gaydosh, S. Padula, A. Garg, T. Biles, and M. Nathal, "Properties and Potential of Two (Ni,Pt)Ti Alloys for Use as High-Temperature Actuator Materials," in *Smart Structures and Materials: Active Materials: Behavior and Mechanics*, included in the current SPIE Conf. Proc. Vol., 2005.
10. K. Otsuka and X. Ren, "Recent developments in the research of shape memory alloys," *Intermetallics* **7**, 511-528, 1999.
11. T. Biggs, L.A. Cornish, M.J. Witcomb, M.B. Cortie, "Revised phase diagram for the Pt-Ti system from 30 to 60% platinum," *J. Alloys Compds.* **375**, 120-127, 2004.
12. A. Garg, unpublished research, NASA Glenn Research Center, 2004.
13. G.W.H. Hohne, W.F. Hemminger, and H.J. Flammersheim, *Differential Scanning Calorimetry*, Springer, Berlin, 116-119, 2003.
14. H.C. Donkersloot and J.H. Van Vucht, "Martensitic Transformations in Gold-Titanium, Palladium-Titanium and Platinum-Titanium Alloys Near the Equiatomic Composition," *J. Less-Common Mets.* **20**, 83-91, 1970.
15. T. Biggs, M.B. Cortie, M.J. Witcomb, and L.A. Cornish, "Martensitic Transformations, Microstructure, and Mechanical Workability of TiPt," *Metall. Maters. Trans. A* **32A**, 1881-1886, 2001.
16. J Ortin and A. Planes, "Thermodynamic Analysis of Thermal Measurements In Thermoelastic Martenstic Transformations," Acta Metall. 36, 1873-1889, 1988.